Article

Reactivity of Perfluorophenyl Azide with Graphene Supported on Cu: Effect of Substrate Crystallinity

Jia Tu and Mingdi Yan *

Department of Chemistry, University of Massachusetts Lowell, Lowell, MA 01854, USA
* Correspondence: mingdi_yan@uml.edu
Received: 1 March 2026; Revised: 14 March 2026; Accepted:16 March; Published: 18 March 2026

Abstract: Effective methods for the covalent functionalization of pristine graphene are limited due to its low chemical reactivity. We developed a covalent chemistry to functionalize graphene using perfluorophenyl azide (PFPA) and demonstrated that the reactivity of graphene can be enhanced by metal substrates. In this work, we investigated the impact of crystalline lattice and morphology of Cu on the reactivity of graphene with PFPA. Graphene grown on single crystalline Cu(111) (Gra/Cu(111)) exhibited the highest degree of functionalization, as evidenced by the largest increase in the D-band intensity obtained from Raman spectroscopy and Raman mapping, along with a low crystallite domain size L_D and a high defect density n_D. In contrast, graphene grown on electropolished polycrystalline Cu (Gra/pCu) showed minimal reactivity toward PFPA reaction. Further Raman analyses demonstrate that Cu(111) induces stronger charge transfer and higher strain in graphene compared to pCu, primarily due to superior lattice matching between graphene and Cu(111), leading to higher reactivity of Gra/Cu(111) toward electron-deficient perfluorophenyl nitrene. Upon transfer of graphene grown on Cu(111) to other substrates, including Cu(111), electropolished pCu, and silicon wafer, the reactivity decreased, and the reactivity of transferred graphene correlates mainly with surface roughness. The decreased reactivity is attributed to weakened graphene–substrate charge interactions after transfer. These findings establish substrate engineering as an effective and non-invasive method for tuning the chemical reactivity of graphene without the need for harsh activation conditions.

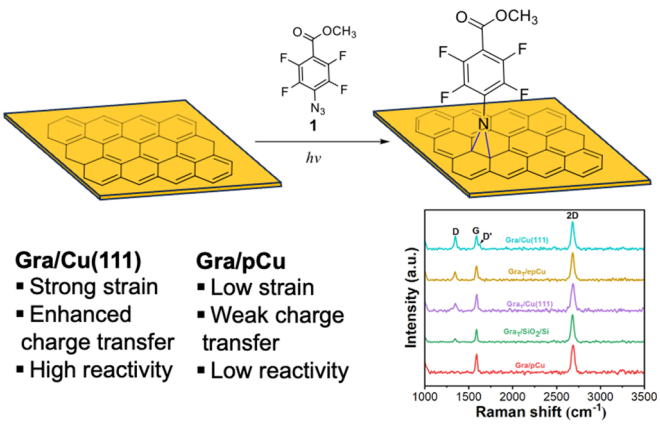

Keywords: graphene; covalent functionalization; perfluorophenyl azide; substrate effect; Cu(111); polycrystalline Cu

1. Introduction

Functionalization of graphene is an important strategy to expand its applications in electronics, sensing, energy storage and biotechnology [1–3]. Various covalent functionalization approaches have been reported, including radical reactions with diazonium salts and peroxides, oxidation, (2+1) cycloadditions with nitrenes, carbenes or malonate derivatives, (2+2) cycloadditions with arynes, (3+2) cycloadditions with azomethine ylides, and (4+2) cycloadditions with dienes or dienophiles [3,4]. Among these, the (2+1) cycloaddition with aryl nitrene is unique in that the reaction can be initiated with UV, heat, or microwave irradiation. Upon the release of N_2, the generated nitrene reacts with graphene to produce covalent adduct. For the reaction of azides with graphene, the (2+1) cycloaddition product aziridine has generally been proposed to be the product structure, analogous to the reaction of azide with other carbon materials such as fullerene [5–7]. However, the exact product structure has not been explicitly confirmed experimentally.

Various azides, including alkyl, silyl, and aryl azides have been used for the covalent functionalization of graphene and highly oriented pyrolytic graphite [8–12]. Literature examples on using azides to functionalize graphene is summarized in Table S1. Compared with perfluorophenyl azides (PFPAs), alkyl, phenyl, and silyl

Copyright: © 2026 by the authors. This is an open access article under the terms and conditions of the Creative Commons Attribution (CC BY) license (https://creativecommons.org/licenses/by/4.0/).
Publisher's Note: Scilight stays neutral with regard to jurisdictional claims in published maps and institutional affiliations.

azides exhibit much lower efficiency. This limitation arises from several intrinsic factors. The short lifetime of singlet nitrenes derived from these azides restricts their ability to engage in productive C-H insertion and cycloaddition reactions [13,14]. Upon photolysis or thermolysis, alkyl and phenyl azides rapidly undergo intersystem crossing (ISC) to the more stable triplet state that is significantly less reactive towards insertion and cycloaddition reactions. In contrast, the strongly electron-withdrawing fluorine atoms of fluorinated aryl azides such as PFPAs suppress ring expansion and ISC, thereby prolonging the singlet nitrene lifetime and enhancing their selectivity toward addition reactions. In the case of silyl azides, steric hindrance plays an important role as silyl azides generate bulky nitrenes in which substituents around the reaction center hinder orbital overlap with graphene's delocalized π network [10,15]. This steric hindrance increases the activation barrier for forming the aziridine ring in the (2+1) cycloaddition, resulting in reduced grafting yields and poor uniformity of functionalization. Safety and stability concerns further limit their practical use [16]. Many alkyl azides are thermally unstable and sensitive to shock or light, posing explosion hazards during synthesis and handling. Silyl azides, while somewhat more stable, are moisture-sensitive and decompose to release toxic gases under ambient conditions. These factors limit reactions with alkyl and silyl azides.

Aryl azides have been increasingly applied in the functionalization of surfaces and nanomaterials, demonstrating remarkable versatility in the covalent functionalization of small organic molecules, polymers, proteins, and carbon materials including fullerenes, carbon tubes, and graphene under ambient, solid state, as well as biological conditions [17,18]. Perfluorophenyl azides (PFPAs) are particularly attractive due to the ease of synthesis from commercially available precursors and the excellent stability under dark conditions. In addition, PFPAs can be readily functionalized with a wide range of reactive groups such as carboxylic acid and its activated esters, e.g., *N*-hydroxysuccinimidyl ester, silanes, phosphates, thiols and disulfide, enabling ready conjugation to both organic and inorganic substrates. Building on these, we and others have employed PFPA chemistry to functionalize graphene to introduce well-defined functional groups, to pattern graphene, and to fabricate graphene-based nanocomposite materials [19–28]. However, the PFPA reaction on graphene typically results in a relatively low degree of functionalization under standard reaction conditions.

Substrate engineering has emerged as a promising strategy in increasing the reactivity of graphene by inducing strain and/or charge doping in the carbon lattice [29,30]. Tensile or compressive strain alters the π-orbital alignment, while charge transfer between graphene and the substrate shifts the Fermi level to favor either electrophilic or nucleophilic reaction. These substrate-induced perturbations directly influence the extent and selectivity of covalent functionalization on graphene. In the reaction with PFPA, computational study revealed that metal-assisted charge transfer lowers the singlet–triplet energy gap, thereby stabilizing the reactive singlet nitrene and enhancing the efficiency of the cycloaddition reaction [21]. Consistent with this prediction, graphene supported on Ni and Cu exhibited higher PFPA reactivity than that on silicon wafer (SiO_2/Si). In this case, the samples were prepared by transferring graphene grown by chemical vapor deposition (CVD) onto polycrystalline Ni and Cu films [21,31].

It has also been reported that the crystal orientation of the metal substrates can influence the reactivity of graphene. For example, graphene grown on single crystalline Cu(111) exhibits higher reactivity than that on polycrystalline Cu (pCu), an effect attributed to substrate-induced strain and charge transfer interactions [32–35]. This substrate-dependent behavior suggests that the crystallographic orientation and morphology of the underlying substrate can be exploited to control the extent of nitrene reaction and thereby fine-tune the degree of covalent functionalization of graphene.

In this work, we investigated how the crystallographic orientation and morphology of the Cu substrate affect the reactivity of graphene toward PFPA functionalization. Graphene was grown via CVD on Cu(111) and pCu. Graphene grown on Cu(111) was also transferred onto Cu(111), electropolished pCu (epCu) and SiO_2/Si (Scheme 1). Using Raman spectroscopy and Raman mapping, we quantified the extent of functionalization and correlated it with substrate-induced strain and charge doping effects. Our results reveal that graphene grown on Cu(111) undergoes the highest degree of functionalization, consistent with its strong substrate coupling with Cu(111). These findings establish substrate crystallography and morphology as an important parameter for tuning the reactivity of graphene towards PFPA reaction.

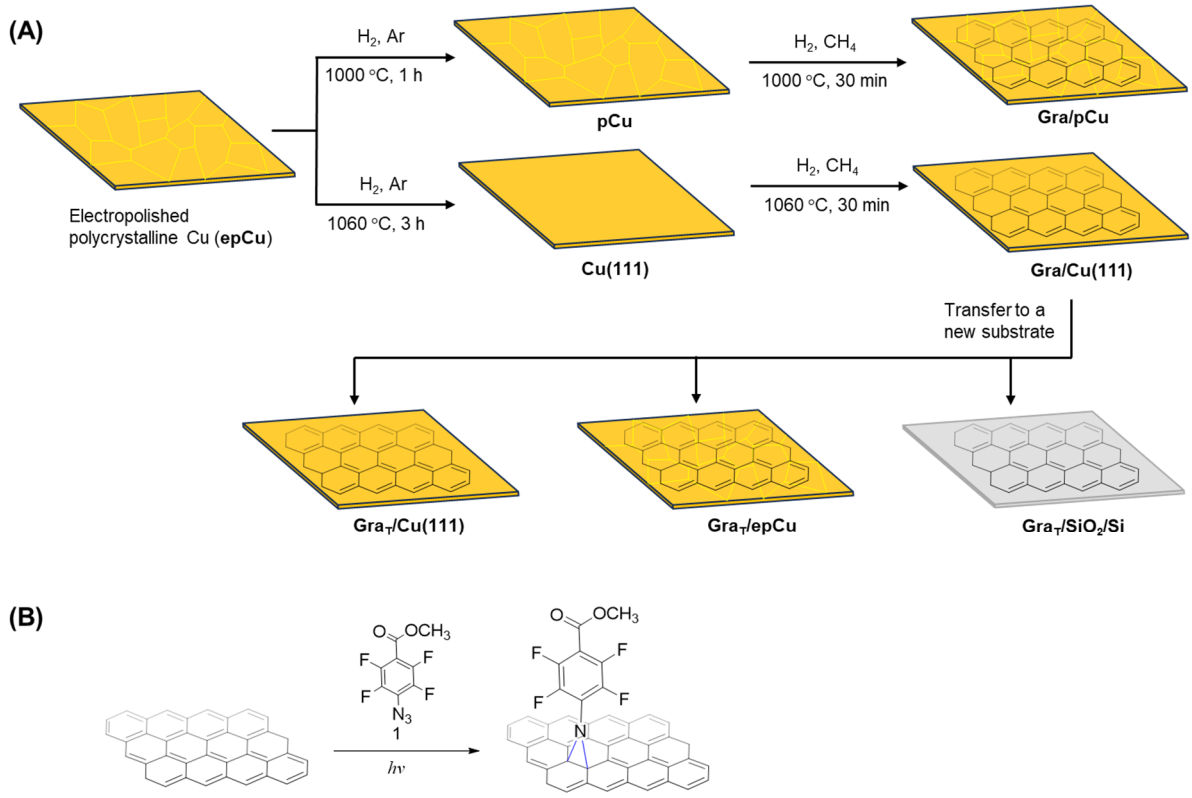

Scheme 1. (**A**) Synthesis of CVD graphene on pCu (Gra/pCu) and on Cu(111) (Gra/Cu(111)), and transfer of graphene grown on Cu(111) to silicon wafer (Gra$_T$/SiO$_2$/Si), electropolished polycrystalline Cu (Gra$_T$/epCu), and Cu(111) (Gra$_T$/Cu(111)). (**B**) Photochemical reaction of graphene with PFPA **1**.

2. Experimental Section

2.1. Materials and Instruments

Copper foils (25 μm thick, annealed, uncoated, 99.8%) and Cu plate (0.675 mm thick, annealed, 99.9%) were purchased from Alfa Aesar (Ward Hill, MA, USA). Silicon wafers with 280 nm thermally grown SiO_2 (single-side polished) were purchased from Fuleda Technology (Wan Chai, China). Ethanol (200 proof) was purchased from Decon Labs, Inc (King of Prussia, PA, USA). Acetone (certified ACS), methanol (certified ACS), isopropanol (>99.5%), and hydrochloric acid (certified ACS Plus) were purchased from Fisher Chemical (Bridgewater, NJ, USA). Urea (99.63%, certified ACS) were purchased from Fisher Chemical (Fair Lawn, NJ, USA) All aqueous solutions were prepared from Milli-Q water (18.2 MΩ·cm). Hydrogen, argon, and methane gases (ultrahigh purity grade) were purchased from Airgas (Billerica, MA, USA). Poly(methyl methacrylate) (PMMA, average molecular weight: 996,000) was purchased from Aldrich Chemical (Milwaukee, WI, USA). Phosphoric acid (>85 wt%) was purchased from Honeywell (USA). Methyl 4-azido-2,3,5,6-tetrafluorobenzoate (PFPA **1**) was synthesized according to a previous procedure [36]. *N*-Methyl-2-pyrrolidone (NMP, anhydrous, 99.5%) and iron(III) chloride (97%) were purchased from Sigma-Aldrich (Milwaukee, WI, USA).

The photochemical reaction was carried out in a UV box equipped with a 450 M medium-pressure mercury lamp. The intensity of the UV lamp was measured to be 36 mW/cm^2 at 280 nm at the location of the reaction using a Coherent FieldMate power meter fitted with a PowerMax PM30 sensor having an active area diameter of 19 mm (Coherent, Inc., Santa Clara, CA, USA). Raman spectra were collected on a Bruker Senterra I spectrometer equipped with a 532 nm laser at the incident power of 1 mW and irradiation time of 10 s. Raman mapping was performed using a HORIBA Scientific Raman microscope equipped with a 532 nm excitation laser. Spectra were acquired with an integration time of 1 s over the range of 1000–3000 cm^{-1}. Each mapping spot covered an area of 2 × 2 μm^2, and a 7 × 7 mapping image (49 spots) was collected for each sample. Atomic force microscopy (AFM) images were obtained using a Bruker Multimode AFM in the tapping mode. Optical images were recorded on a Nikon ECLIPSE L200 microscope using a Moticam 2500 camera. X-ray diffraction (XRD) analysis was carried out on a Rigaku MiniFlex 600 diffractometer equipped with Cu Kα radiation (λ = 1.5418 Å).

2.2. Fabrication of Graphene on pCu and Cu(111)

Monolayer graphene was synthesized by CVD on both pCu and Cu(111) following a previous procedure [37]. The substrates were prepared from commercial Cu foils that were electropolished to remove surface oxides and reduce surface roughness. Electropolishing was carried out by using commercial Cu foils as the anode and a copper plate as the cathode at a constant current of 2.8 A for 180 s. The electropolishing solution was prepared from a stock solution containing 1000 mL of Milli-Q water, 500 mL of phosphoric acid, 500 mL of ethanol, 100 mL of isopropyl alcohol, and 10.0 g of urea. After electropolishing, the Cu foils were thoroughly rinsed with water, ethanol, and acetone, and then dried under an argon stream to give epCu.

To synthesize Gra/pCu, the electropolished Cu foil was first annealed at 1000 °C in a homebuilt CVD furnace [37] under a flow of H_2 (10 sccm) and Ar (~15 sccm) for 1 h to give pCu (Scheme 1). After annealing, the argon valve was closed, and CH_4 (3–6 sccm) was introduced while maintaining the H_2 flow at 10 sccm. Graphene was grown at 1000 °C for 30 min. The furnace was then rapidly cooled to ~50 °C under a continuous flow of H_2 and CH_4, after which the gases were turned off and the chamber was open to ambient environment.

To synthesize Gra/Cu(111), the electropolished Cu foil was annealed at 1060 °C for 3 h under a flow of H_2 (10 sccm) and argon (~15 sccm) to produce Cu(111) (Scheme 1). Graphene growth on Cu(111) was carried out in the same manner as for pCu except at the growth temperature of 1060 °C.

2.3. Transfer of Graphene onto SiO_2/Si, epCu, and Cu(111)

Graphene grown on Cu(111) was transferred to silicon wafer (SiO_2/Si), epCu, and Cu(111) using the PMMA-assisted wet-transfer method [38]. Briefly, a solution of PMMA in acetone (40 mg/mL) was spin-coated on the side of graphene at 1000 rpm for 1 min. The Cu foil was then etched away in a $FeCl_3$/HCl (1 M $FeCl_3$ in 3 M HCl) for 3 h. The PMMA-supported graphene film was rinsed thoroughly in 1 M HCl solution followed by Milli-Q water several times. PMMA-supported graphene was then scooped from Milli-Q water onto the target substrate. After drying at room temperature, the sample was immersed in acetone for 3 h, repeated once more to obtain a clean graphene film on the target substrate, yielding $Gra_T/SiO_2/Si$, Gra_T/epCu, and Gra_T/Cu(111) (Scheme 1).

2.4. Reaction of Graphene with PFPA

Graphene supported on different substrates was immersed in an anhydrous NMP solution of PFPA **1** (0.1 M). The sample was then irradiated with a 450 M medium-pressure mercury lamp through a 280-nm long-pass optical filter at room temperature for 40 min. After irradiation, the sample was rinsed with acetone three times. Except for $Gra_T/SiO_2/Si$ which was used directly for Raman characterization, other samples were transferred onto silicon wafer prior to Raman characterization.

2.5. Characterization by Raman Spectroscopy and Mapping

For each sample, Raman spectra were collected from randomly selected 76–246 points across the graphene surface to account for spatial inhomogeneity. The peak height of D (~1350 cm^{-1}) and G (~1590 cm^{-1}) bands was used to calculate peak intensity and I_D/I_G. Crystallite domain size (L_D) and defect density (n_D) were calculated using the Tuinstra–Koenig relation [21]. The relative change in I_D/I_G ($\Delta I_D/I_G$) before and after reaction was quantified as

$$\Delta I_D/I_G = \frac{(I_D/I_G)_{\text{after}} - (I_D/I_G)_{\text{before}}}{(I_D/I_G)_{\text{before}}} \times 100$$

3. Results

3.1. Preparation of Monolayer Graphene on Various Substrates

Monolayer graphene on Cu(111) (Gra/Cu(111)) or pCu (Gra/pCu) was prepared in a home-build CVD setup following the protocol developed previously [37]. In the process, commercial polycrystalline copper foils were first subjected to electropolishing to remove surface contaminants and reduce surface roughness, yielding epCu. The foils were then annealed in the furnace at 1000 °C for 1 h or at 1060 °C for 3 h to give pCu or single crystal Cu(111), respectively (Scheme 1). The XRD pattern of commercial pCu, electropolished pCu and annealed pCu all shows multiple prominent diffraction peaks corresponding to (331), (111), (220), and (200) facets, with the (331) being the most intense (Figure 1). On the other hand, as-prepared Cu(111) foil contains a single sharp diffraction peak corresponding to the (111) facet. To grow graphene, annealed pCu and Cu(111) foils were exposed

to 10 sccm H_2 and 3–6 sccm CH_4 at 1000 °C or 1060 °C for 30 min to give Gra/pCu or Gra/Cu(111), respectively. Graphene transferred to other substrates was prepared by transferring Gra/Cu(111) to silicon wafer, epCu, or Cu(111) by PMMA-assisted wet transfer to give $Gra_T/SiO_2/Si$, Gra_T/epCu, and Gra_T/Cu(111) (Scheme 1).

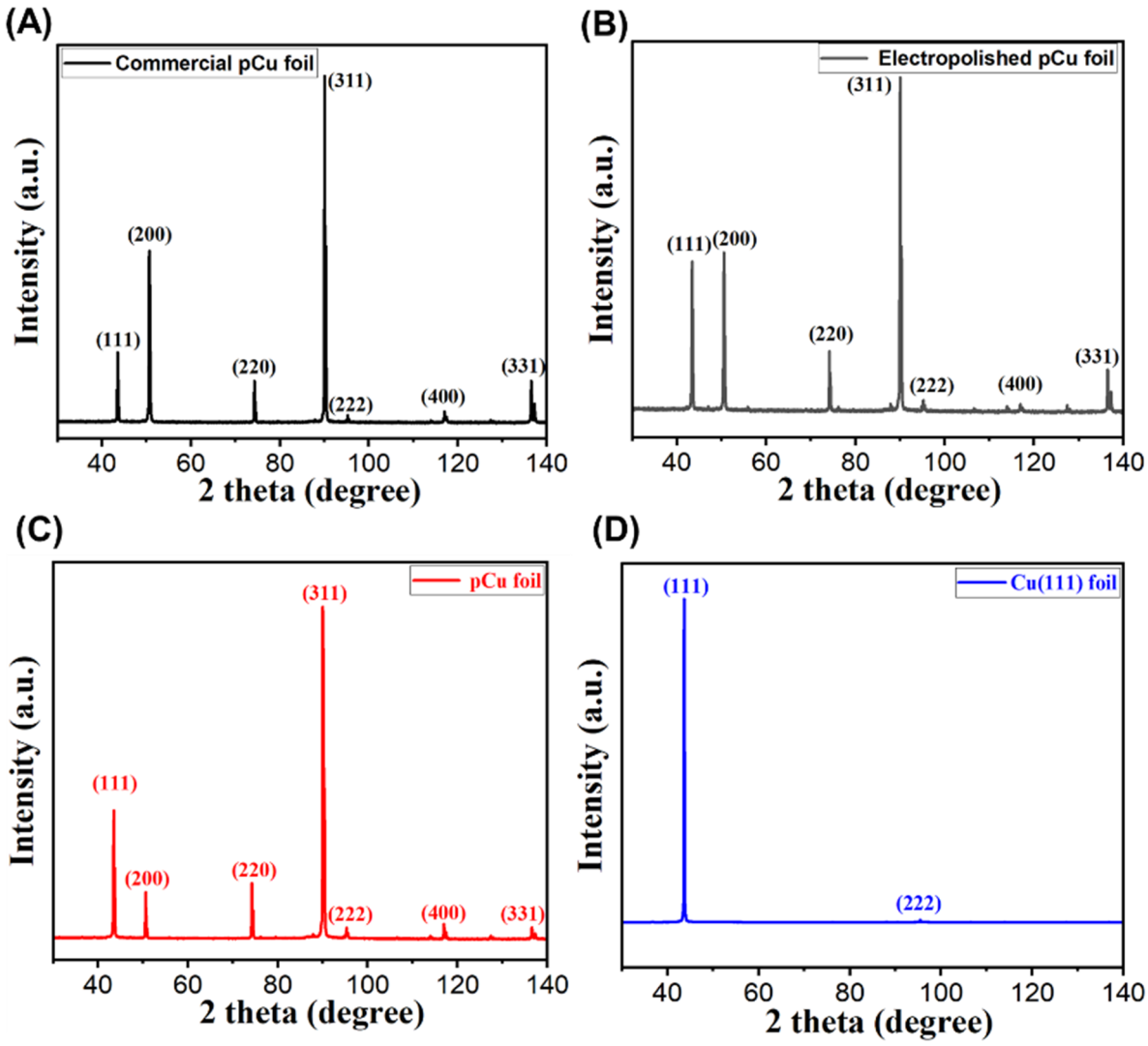

Figure 1. XRD patterns of (**A**) as-received polycrystalline copper foil, (**B**) electropolished polycrystalline copper foil (epCu) (**C**) electropolished polycrystalline copper foil annealed in H_2/Ar at 1000 °C for 1 h (pCu), and (**D**) Cu(111) foil.

3.2. Functionalization of Graphene on Different Substrates

Reactions were carried out by immersing graphene samples in 0.1 M solution of PFPA in anhydrous NMP, covered the vial with a 280-nm long-pass filter, and then irradiated with a medium-pressure Hg lamp at room temperature for 40 min. The irradiation time was selected based on our previous systematic investigation of PFPA reactions with graphene [21]. We have also demonstrated that without PFPA, irradiating graphene in NMP under identical conditions showed no increase in the Raman D band intensity, indicating that neither NMP nor UV irradiation introduces detectable defects in graphene under the reaction conditions [21]. After extensive rinsing with acetone and drying, graphene supported on Cu was transferred onto silicon wafer, and Raman spectra were collected. The as-grown Gra/pCu (Figure S1A) and Gra/Cu(111) (Figure S2A) showed the characteristic single layer graphene features of symmetric 2D peak and $I_{2D}/I_G > 2$, as well as minimal D band, indicative of minimal structural defects in the as-prepared unfunctionalized graphene. After reaction with PFPA, all functionalized graphene samples (Figure 2A) exhibit defect-related D bands at ~1350 cm^{-1} with varying intensities reflecting different extents of defect incorporation [29,39]. After functionalization, Gra/Cu(111) shows the most pronounced D peak together with a D' band at ~1625 cm^{-1} (Figures 2A and S2B). The D band arises from defect-activated intervalley scattering, whereas D' band originates from intravalley scattering and is particularly sensitive to localized point-like sp^3 defects [40,41]. The simultaneous presence of D and D' bands indicate localized symmetry-breaking defects introduced by PFFA

functionalization of graphene. In contrast, Gra/pCu shows the weakest D-band intensity (Figures 2A and S1B). The transferred samples ($Gra_T/SiO_2/Si$, Gra_T/epCu, and Gra_T/Cu(111)) exhibit intermediate D-band intensities, following the trend Gra_T/Cu(111) > Gra_T/epCu > $Gra_T/SiO_2/Si$ (Figures 2A and S2C–E).

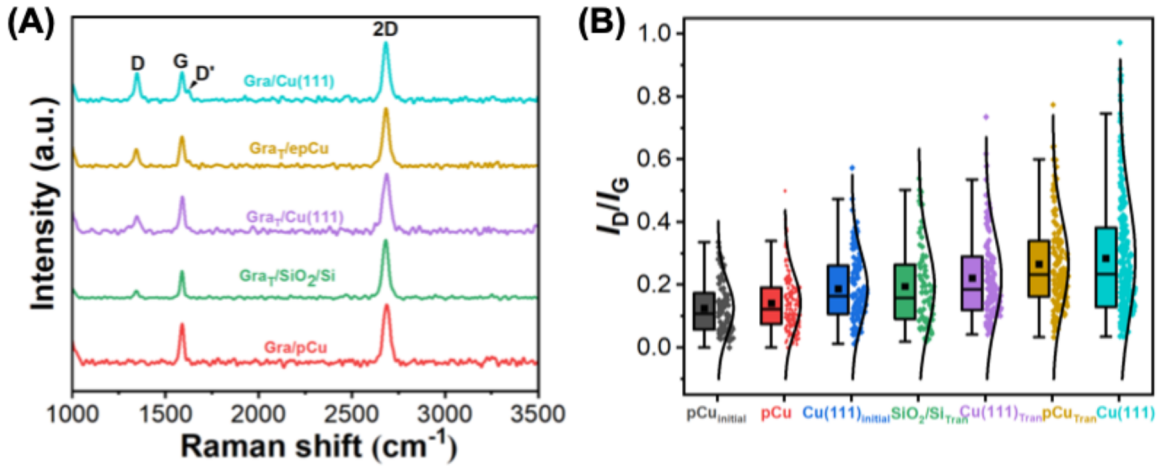

(C)

Sample	Condition	I_D/I_G	$\%\Delta I_D/I_G$	L_D (nm)	n_D (×10^9 cm^{-2})
Gra/pCu	Initial	0.13 ± 0.08	--	41 ± 16	28 ± 18
	After reaction	0.14 ± 0.09	7.7%	38 ± 16	32 ± 20
Gra/Cu(111)	Initial	0.18 ± 0.11	--	33 ± 13	42 ± 24
Gra$_T$/SiO$_2$/Si	After reaction	0.19 ± 0.14	5.6%	33 ± 14	43 ± 30
Gra$_T$/Cu(111)		0.22 ± 0.14	22%	29 ± 9.1	49 ± 30
Gra$_T$/epCu		0.27 ± 0.15	50%	26 ± 8.6	59 ± 32
Gra/Cu(111)		0.28 ± 0.19	56%	27 ± 10	63 ± 43

Figure 2. Raman analysis of graphene supported on different substrates after reaction with PFPA. (**A**) Typical Raman spectra of PFPA-functionalized Gra/Cu(111), Gra_T/epCu, Gra_T/Cu(111), $Gra_T/SiO_2/Si$, and Gra/pCu. Additional Raman spectra can be found in Figures S1B and S2B–E. (**B**) Box-violin plots showing the distribution of I_D/I_G for PFPA-functionalized graphene samples. The boxes represent the interquartile range (25th–75th percentile), with whiskers indicating the data spread. The surrounding violin plots show the full probability distribution of the data, obtained from 82 (Gra/pCu$_{initial}$), 210 (Gra/pCu), 112 (Gra/Cu(111)$_{initial}$), 76 ($Gra_T/SiO_2/Si$), 145 (Gra/Cu(111)), 130 (Gra_T/epCu), and 246 (Gra/Cu(111)) Raman spectra, respectively. (**C**) Raman-derived parameters, I_D/I_G, $\%\Delta I_D/I_G$, L_D, and n_D, of graphene samples before and after reaction with PFPA. The L_D, and n_D calculations can be found in Supplementary Materials. Data are presented as mean ± standard deviation.

Further Raman analyses (Figure 2C) show that after reaction with PFPA, the relative change in I_D/I_G, $\%\Delta I_D/I_G$, was 7.7% for Gra/pCu. On the other hand, I_D/I_G of Gra/Cu(111) increased substantially to $\Delta I_D/I_G$ of 56% after reaction with PFPA. The transferred graphene samples show intermediate increase in $\Delta I_D/I_G$, at 5.6%, 22%, and 50% for $Gra_T/SiO_2/Si$, Gra_T/Cu(111), and Gra_T/epCu, respectively. Overall, the extent of defect incorporation follows the trend of Gra/Cu(111) > Gra_T/epCu > Gra_T/Cu(111) > Gra/pCu ≈ $Gra_T/SiO_2/Si$, with Gra/Cu(111) having the highest degree of defect incorporation.

Raman mapping of I_D/I_G was performed to visualize the spatial distribution of PFPA functionalization of graphene across graphene supported on different substrates (Figure 3). Consistent with the Raman spectroscopy data in Figure 2, as-prepared Gra/pCu (Gra/pCu$_{initial}$) exhibits a low and spatially uniform I_D/I_G of 0.13 ± 0.03, which increases only marginally to 0.14 ± 0.02 after PFPA functionalization, indicating minimal structural modification. Similarly, as-prepared Gra/Cu(111) (Gra/Cu(111)$_{initial}$) shows a low average I_D/I_G of 0.16 ± 0.03. After PFPA functionalization, a high I_D/I_G of 0.34 ± 0.13 is observed for Gra/Cu(111), together with localized regions of significantly increased I_D/I_G, indicating that graphene directly grown on Cu(111) undergoes the most extensive functionalization. $Gra_T/SiO_2/Si$ displays a small increase in I_D/I_G to 0.19 ± 0.05, whereas Gra_T/Cu(111) shows a modest increase in I_D/I_G to 0.24 ± 0.10. More pronounced increase in I_D/I_G was observed for Gra_T/epCu, which exhibits an elevated I_D/I_G of 0.29 ± 0.17.

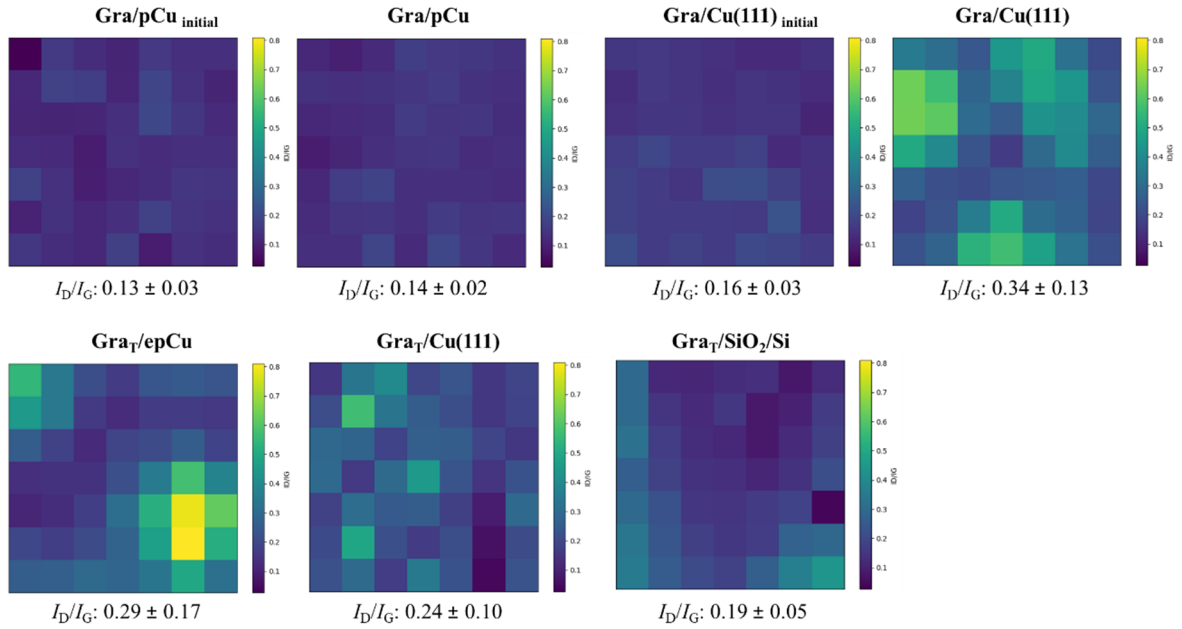

Figure 3. Raman I_D/I_G mapping of graphene on different substrates before (initial) and after PFPA functionalization. Each Raman mapping spot corresponds to an area of 2 × 2 μm^2.

3.3. Extent of Functionalization

To quantify the extent of functionalization, statistical analyses of crystallite domain size (L_D) and defect density (n_D) [40,41] were performed and results are shown in Figure 3C. Here, L_D represents the average distance between neighboring point defects, while n_D denotes the number of defects per area and is inversely proportional to L_D^2. Figure 4A shows box violin plots of L_D for all samples, showing the data as well as statistical distribution. The as-prepared Gra/pCu and Gra/Cu(111) exhibit relatively large L_D values (41 ± 16 nm and 33 ± 13 nm, respectively), indicating large crystallite domain size. After PFPA functionalization, L_D decreases slightly for Gra/pCu (38 ± 16 nm) but more significantly for Gra/Cu(111) (27 ± 10 nm), indicating enhanced defect incorporation on Gra/Cu(111). Transferred samples also show reduced domain sizes, with Gra$_T$/epCu and Gra$_T$/Cu(111) yielding L_D values of 26 ± 8.6 nm and 29 ± 9.1 nm, respectively. In contrast, Gra/SiO$_2$/Si shows only a minimal change (33 ± 14 nm), consistent with its relatively low reactivity. These results clearly demonstrate that smaller domain sizes correlate with higher extent of functionalization. Particularly, Gra/Cu(111) with the smallest L_D reflects its strong substrate–graphene interaction that facilitates reaction with PFPA.

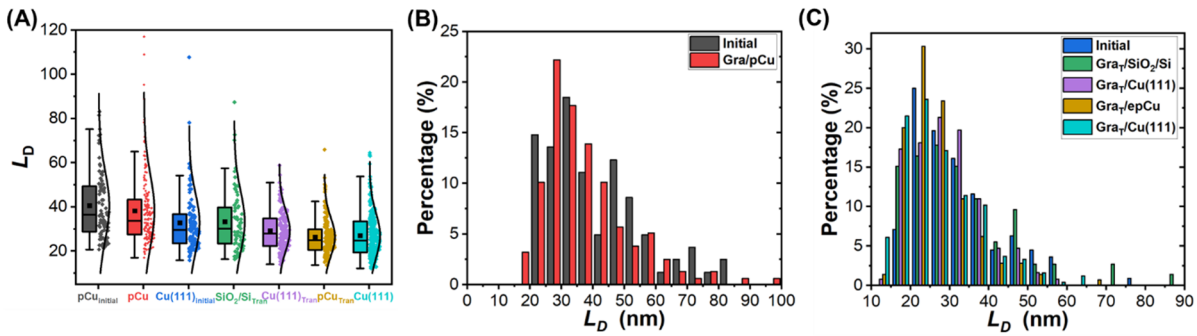

Figure 4. Statistical analysis of crystallite domain size (L_D) in graphene on different substrates before and after PFPA functionalization. (**A**) Box–violin plots of L_D distribution. (**B**) Histograms of L_D values for Gra/pCu before (grey), and after PFPA functionalization (red). (**C**) Histograms of L_D values for Gra/Cu(111) before (blue), and after PFPA functionalization (turquois), and after PFPA functionalization for Gra$_T$/SiO$_2$/Si (green), Gra$_T$/Cu(111) (purple), and Gra$_T$/epCu (gold).

The defect density (n_D) was also analyzed, and the results are shown in Figure 5. The as-prepared Gra/pCu shows the lowest defect density ((28.1 ± 18.5) × 10^9 cm^{-2}), while as-prepared Gra/Cu(111) exhibits a slightly higher n_D ((41.5 ± 24.5) × 10^9 cm^{-2}). Following functionalization, the defect density increases across all substrates,

with the most pronounced increase observed for Gra/Cu(111), reaching (62.7 ± 42.9) × 10^9 cm^{-2}), followed closely by Gra$_T$/epCu ((58.7 ± 32.1) × 10^9 cm^{-2}). Gra$_T$/Cu(111) and Gra$_T$/SiO_2/Si exhibit more modest increases at (49.0 ± 30.3) × 10^9 cm^{-2} and (43.1 ± 29.5) × 10^9 cm^{-2}, respectively. Gra/pCu shows a slight increase to (31.5 ± 19.9) × 10^9 cm^{-2}. Overall, the combined L_D and n_D analyses reinforce the conclusion that graphene grown on Cu(111) is the most reactive toward PFPA functionalization, while graphene grown on pCu is the least reactive. Transferred samples exhibit intermediate reactivities, indicating partial retention of substrate-induced effects after transfer.

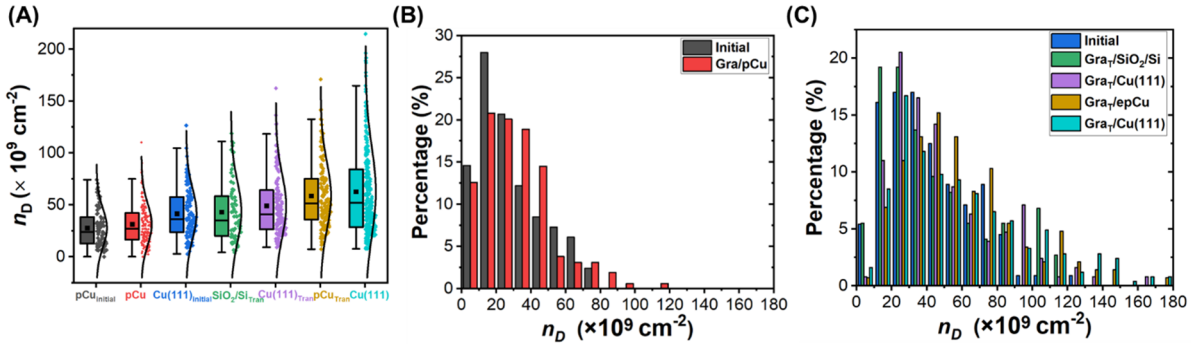

Figure 5. Statistical analysis of defect density (n_D) in graphene on different substrates before and after PFPA functionalization. (**A**) Box violin plots of n_D distribution. (**B**) Histograms of n_D values for Gra/pCu before (grey), and after PFPA functionalization (red). (**C**) Histograms of L_D values for Gra/Cu(111) before (blue), and after PFPA functionalization (turquois), and after PFPA functionalization for Gra$_T$/SiO_2/Si (green), Gra$_T$/Cu(111) (purple), and Gra$_T$/epCu (gold).

4. Discussions

Collectively, the results reveal a clear substrate-dependent reactivity of graphene toward PFPA functionalization. Graphene grown on pCu and Cu(111) exhibits markedly different reactivity toward PFPA functionalization. Gra/Cu(111) showed the highest reactivity, whereas Gra/pCu showed minimal reactivity. Transfer partially diminished or redistributed this reactivity, with transferred graphene on epCu displaying the most significant reactivity among the transferred samples. Below, we discuss the possible reasons for the overall reactivity trend: Gra/pCu < Gra$_T$/SiO_2/Si < Gra$_T$/Cu(111) < Gra$_T$/epCu < Gra/Cu(111).

4.1. Substrate-Induced Strain and Doping Effects

The Raman features of graphene grown on polycrystalline Cu and monocrystalline Cu(111) were compared. The correlation of G- and 2D-band positions (Figure 6A) reveals upshift for Gra/Cu(111) relative to Gra/pCu. The centroids for both bands also shift toward higher wavenumbers. These shifts are shown in the representative spectra in Figure 6B,C), where both the G and 2D bands for Gra/Cu(111) appear at higher wavenumbers than for Gra/pCu.

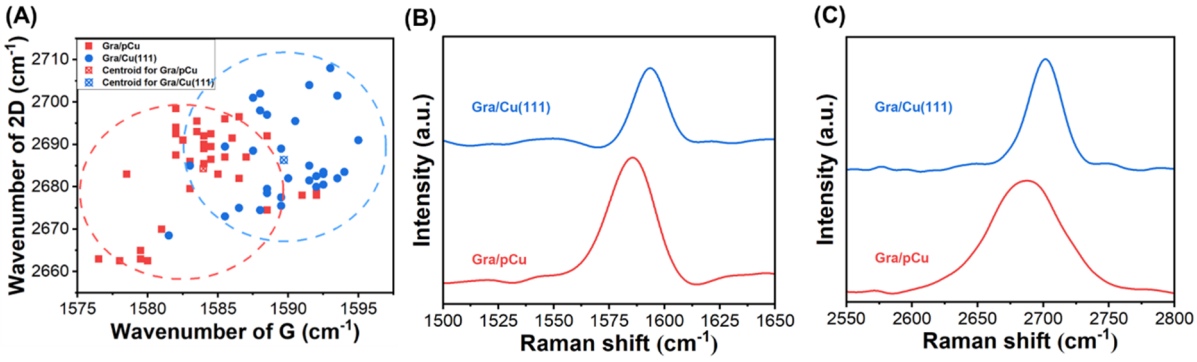

Figure 6. Raman spectral analysis of graphene grown on polycrystalline Cu and monocrystalline Cu(111). (**A**) Correlation plot of G- and 2D-band positions, with the centroid indicated as a red and a blue cross for Gra/pCu and Gra/Cu(111), respectively. Representative (**B**) G-band, and (**C**) 2D-band spectra highlighting the distinct peak positions.

Such wavenumber upshifts in the G and 2D modes are characteristic signatures of substrate-induced effects [33,35,42,43]. The upshifted G band indicates enhanced n-type doping due to stronger charge transfer from Cu(111) to graphene, while the upshifted 2D band suggests compressive strain arising from the epitaxial

relationship and better lattice matching between graphene and the Cu(111) substrate. In contrast, graphene on pCu exhibits comparatively lower band positions, consistent with weaker substrate coupling and less pronounced electronic or strain modulation. These results demonstrate that Cu(111) induces stronger substrate interactions, leading to greater charge transfer and strain effects compared to polycrystalline Cu, thereby contributing to the enhanced reactivity of Gra/Cu(111) observed during PFPA functionalization [33,35].

4.2. Morphology of Graphene on Various Substrates

Optical microscopy and AFM imaging both reveal distinct surface characteristics of graphene grown on pCu and Cu(111). As shown in Figure 7A, Gra/pCu exhibits rough and nonuniform morphology with an average AFM root mean square (RMS) roughness of 8.23 ± 0.92 nm. In contrast, Gra/Cu(111) displays smooth, relatively ordered surface morphology with RMS roughness of 1.87 ± 0.29 nm. From the larger area optical microscopy images, Gra/pCu surface shows interconnected network of grain boundaries (Figure 7A), whereas Gra/Cu(111) appears continuous and shows more homogeneous surface (Figure 7B). As the surface curvature could also lead to enhanced reactivity, the higher reactivity of Gra/Cu(111) than that of Gra/pCu toward PFPA reaction is therefore attributed to charge doping and strain [21,29,44–49].

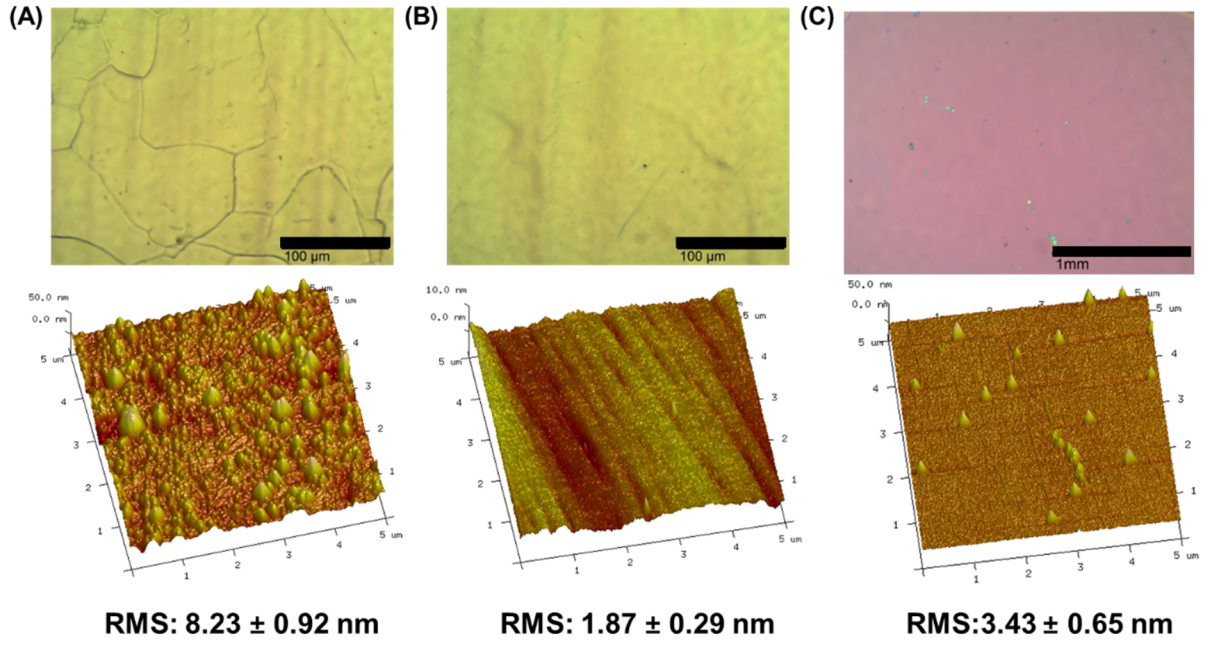

Figure 7. Optical microscopy (**top**) and AFM (**bottom**) images of (**A**) Gra/pCu, (**B**) Gra/Cu(111), and (**C**) $Gra_T/SiO_2/Si$. Additional images can be found in Figures S3 and S4.

For the transferred samples, the graphene morphology is governed by the surface morphology of the supporting substrates through conformal adhesion [44,50–53]. The RMS roughness values of Gra/epCu and Gra/Cu(111) were measured previously as 38.8 ± 12 nm and 21.0 ± 4.2 nm, respectively [37], and $Gra_T/SiO_2/Si$ shows a uniform, continuous graphene film with a significantly lower RMS roughness of 3.43 ± 0.65 nm (Figure 7C). These results indicate a correlation between the reactivity of transferred graphene and the roughness of the supporting substrates. Specifically, the higher surface roughness of Gra/epCu induces greater graphene corrugation, leading to enhanced reactivity of GraT/epCu among the transferred samples. As the substrate roughness decreases, the reactivity decreases, as observed for $Gra_T/Cu(111)$ and $Gra_T/SiO_2/Si$. Despite retaining the Cu(111) crystallographic orientation, $Gra_T/Cu(111)$ exhibits lower reactivity than $Gra_T/epCu$, which can be attributed to weaker graphene–substrate charge interaction in $Gra_T/Cu(111)$ after transfer, leading to reduced strain and charge-doping effects. In contrast, $Gra/SiO_2/Si$ shows the lowest reactivity, attributed to reduced surface roughness and/or distribution of charge puddles that passivates graphene reactivity [21,29,43]. Thus, for transferred substrates, graphene reactivity toward PFPA correlates with graphene roughness.

5. Conclusions

In this work, we carried out the photochemical reaction of PFPA with graphene on different substrates and investigated the role of supporting substrates in modulating graphene reactivity. Graphene grown on Cu(111)

exhibited the highest degree of functionalization, as evidenced by the largest increase in $\Delta I_D/I_G$ obtained from Raman spectroscopy and Raman mapping, along with decrease in L_D and increase in n_D. In contrast, graphene grown on polycrystalline Cu showed minimal reactivity toward PFPA reaction. Raman analyses further demonstrate that Cu(111) induces stronger charge transfer and higher strain in graphene compared to pCu, primarily due to superior lattice matching between graphene and the Cu(111) surface. These substrate-induced electronic and structural effects enhance graphene's reactivity toward the electron-deficient perfluorophenyl nitrene, leading to higher reactivity.

Upon transfer of graphene grown on Cu(111) to other substrates, including Cu(111), electropolished pCu, and SiO_2/Si, the reactivity decreased. The decreased reactivity is attributed to weakened graphene–substrate charge interactions after transfer, and the reactivity of transferred graphene correlates mainly with the surface roughness.

Overall, these findings establish substrate engineering as an effective and non-invasive method for tuning the chemical reactivity of graphene without the need for harsh activation conditions. By leveraging the intrinsic interaction between graphene and the substrate, this approach enables controlled covalent functionalization of graphene, offering a versatile approach for chemical modification of graphene.

Supplementary Materials: The following supporting information can be downloaded at: https://media.sciltp.com/articles/others/260318122437075 7/MI-26030002_Supplementary_Materials.pdf. Reference [54] is cited in the Supplementary Materials.

Author Contributions: J.T.: conceptualization, methodology, software, data curation, writing—original draft preparation, visualization, investigation, and validation; M.Y.: conceptualization, methodology, data curation, visualization, supervision, software, validation, writing—reviewing and editing. All authors have read and agreed to the published version of the manuscript.

Funding: The authors are grateful for the financial support from the National Science Foundation (CHE-2305006).

Data Availability Statement: Not applicable.

Acknowledgments: The authors thank Ji-Xin Cheng and Bethany Weinberg of Boston University for their kind help in Raman mapping.

Conflicts of Interest: The authors declare no conflict of interest.

Use of AI and AI-Assisted Technologies: During the preparation of this work, the authors used ChatGPT to assist with language editing of the manuscript. The authors reviewed and edited the content as necessary and take full responsibility for the content of the published article.

References

1. Liu, J.; Tang, J.; Gooding, J.J. Strategies for chemical modification of graphene and applications of chemically modified graphene. *J. Mater. Chem.* **2012**, *22*, 12435–12452.
2. Park, J.; Yan, M. Covalent functionalization of graphene with reactive intermediates. *Acc. Chem. Res.* **2013**, *46*, 181–189.
3. Stergiou, A.; Cantón-Vitoria, R.; Psarrou, M.N.; Economopoulos, S.P.; Tagmatarchis, N. Functionalized graphene and targeted applications–Highlighting the road from chemistry to applications. *Prog. Mater Sci.* **2020**, *114*, 100683.
4. Chua, C.K.; Pumera, M. Covalent chemistry on graphene. *Chem. Soc. Rev.* **2013**, *42*, 3222–3233.
5. Yan, M.; Cai, S.X.; Keana, J.F.W. Photochemical and Thermal Reactions of C60 with N-Succinimidyl 4-Azido-2,3,5,6-tetrafluorobenzoate: A New Method for Functionalization of C60. *J. Org. Chem.* **2002**, *59*, 5951–5954.
6. Liu, F.; Du, W.; Liang, Q.; Wang, Y.; Zhang, J.; Zhao, J.; Zhu, S. Synthesis of 4-aziridino[C60]fullerene-1,8-naphthalimide (C60-NI dyads) and their photophysical properties. *Tetrahedron* **2010**, *66*, 5467–5471.
7. Khalilov, M.; Tulyabaev, A.R.; Akhmetov, A.R.; Tuktarov, A.R. Synthesis and ^{13}C NMR features of N-substituted aziridino[60]fullerenes. *Russ. Chem. Bull.* **2016**, *64*, 2725–2730.
8. Gross, A.J.; Yu, S.S.; Downard, A.J. Two-component mixed and patterned films on carbon surfaces through the photografting of arylazides. *Langmuir* **2010**, *26*, 7285–7292.
9. Tanaka, M.; Sawaguchi, T.; Sato, Y.; Yoshioka, K.; Niwa, O. Surface modification of GC and HOPG with diazonium, amine, azide, and olefin derivatives. *Langmuir* **2011**, *27*, 170–178.
10. Choi, J.; Kim, K.-j.; Kim, B.; Lee, H.; Kim, S. Covalent functionalization of epitaxial graphene by azidotrimethylsilane. *J. Phys. Chem. C* **2009**, *113*, 9433–9435.
11. Strom, T.A.; Dillon, E.P.; Hamilton, C.E.; Barron, A.R. Nitrene addition to exfoliated graphene: A one-step route to highly functionalized graphene. *Chem. Commun.* **2010**, *46*, 4097–4099.
12. Vadukumpully, S.; Gupta, J.; Zhang, Y.; Xu, G.Q.; Valiyaveettil, S. Functionalization of surfactant wrapped graphene nanosheets with alkylazides for enhanced dispersibility. *Nanoscale* **2011**, *3*, 303–308.
13. Poe, R.; Schnapp, K.; Young, M.J.; Grayzar, J.; Platz, M.S. Chemistry and kinetics of singlet pentafluorophenylnitrene. *J. Am. Chem. Soc.* **1992**, *114*, 5054–5067.

14. Kotzyba-Hibert, F.; Kapfer, I.; Goeldner, M. Recent trends in photoaffinity labeling. *Angew. Chem. Int. Ed.* **1995**, *34*, 1296–1312.
15. Denis, P.A.; Iribarne, F. Monolayer and bilayer graphene functionalized with nitrene radicals. *J. Phys. Chem. C* **2011**, *115*, 195–203.
16. Bräse, S.; Gil, C.; Knepper, K.; Zimmermann, V. Organic azides: An exploding diversity of a unique class of compounds. *Angew. Chem. Int. Ed.* **2005**, *44*, 5188–5240.
17. Wang, X.; Liu, L.H.; Ramstrom, O.; Yan, M. Engineering nanomaterial surfaces for biomedical applications. *Exp. Biol. Med.* **2009**, *234*, 1128–1139.
18. Liu, L.H.; Yan, M. Perfluorophenyl azides: New applications in surface functionalization and nanomaterial synthesis. *Acc. Chem. Res.* **2010**, *43*, 1434–1443.
19. Liu, L.-H.; Yan, M. Functionalization of pristine graphene with perfluorophenyl azides. *J. Mater. Chem.* **2011**, *21*, 3273–3276.
20. Nagel, T.; Jurkiewicz, L.; Hauke, F.; Hirsch, A. Laser-Initiated Covalent Functionalization of Graphene Using Perfluorophenylazides with Local Addend-Binding Control. *Phys. Status Solidi Basic Res.* **2025**, *263*, 2500348.
21. Yang, X.; Chen, F.; Kim, M.A.; Liu, H.; Wolf, L.M.; Yan, M. On the Reactivity Enhancement of Graphene by Metallic Substrates towards Aryl Nitrene Cycloadditions. *Chem. Eur. J.* **2021**, *27*, 7887–7896.
22. Park, J.; Yang, X.; Wickramasinghe, D.; Sundhoro, M.; Orbey, N.; Chow, K.F.; Yan, M. Functionalization of pristine graphene for the synthesis of covalent graphene-polyaniline nanocomposite. *RSC Adv.* **2020**, *10*, 26486–26493.
23. Park, J.; Jin, T.; Liu, C.; Li, G.; Yan, M. Three-dimensional graphene–TiO_2 nanocomposite photocatalyst synthesized by covalent attachment. *ACS Omega* **2016**, *1*, 351–356.
24. Liu, L.-H.; Yan, M. Simple method for the covalent immobilization of graphene. *Nano Lett.* **2009**, *9*, 3375–3378.
25. Liu, L.-H.; Zorn, G.; Castner, D.G.; Solanki, R.; Lerner, M.M.; Yan, M. A simple and scalable route to wafer-size patterned graphene. *J. Mater. Chem.* **2010**, *20*, 5041–5046.
26. Park, J.; Jayawardena, H.S.N.; Chen, X.; Jayawardana, K.W.; Sundhoro, M.; Ada, E.; Yan, M. A general method for the fabrication of graphene–nanoparticle hybrid material. *Chem. Commun.* **2015**, *51*, 2882–2885.
27. Kong, N.; Park, J.; Yang, X.; Ramström, O.; Yan, M. Carbohydrate functionalization of few-layer graphene through microwave-assisted reaction of perfluorophenyl azide. *ACS Appl. Bio Mater.* **2018**, *2*, 284–291.
28. Liu, L.-H.; Lerner, M.M.; Yan, M. Derivitization of pristine graphene with well-defined chemical functionalities. *Nano Lett.* **2010**, *10*, 3754–3756.
29. Tu, J.; Yan, M. Enhancing the Chemical Reactivity of Graphene through Substrate Engineering. *Small* **2024**, *2024*, e2408116.
30. Criado, A.; Melchionna, M.; Marchesan, S.; Prato, M. The Covalent Functionalization of Graphene on Substrates. *Angew. Chem. Int. Ed.* **2015**, *54*, 10734–10750.
31. Yang, X.; Chen, F.; Kim, M.A.; Liu, H.; Wolf, L.M.; Yan, M. Using metal substrates to enhance the reactivity of graphene towards Diels-Alder reactions. *Phys. Chem. Chem. Phys.* **2022**, *24*, 20082–20093.
32. Tu, J.; Zhou, W.; Wolf, L.M.; Yan, M. Inverse-Electron-Demand Diels-Alder Reaction of Tropone with Graphene Supported on Cu(111). *Small* **2025**, *21*, e03669.
33. Zhang, X.; Luo, D.; Zhang, H.; Hwang, D.Y.; Park, S.O.; Li, B.-W.; Biswal, M.; Jiang, Y.; Huang, Y.; Kwak, S.K. Effect of copper substrate surface orientation on the reductive functionalization of graphene. *Chem. Mater.* **2019**, *31*, 8639–8648.
34. Plsek, J.; Kovaricek, P.; Vales, V.; Kalbac, M. Tuning the Reactivity of Graphene by Surface Phase Orientation. *Chem. Eur. J.* **2017**, *23*, 1839–1845.
35. Li, B.W.; Luo, D.; Zhu, L.; Zhang, X.; Jin, S.; Huang, M.; Ding, F.; Ruoff, R.S. Orientation-Dependent Strain Relaxation and Chemical Functionalization of Graphene on a Cu(111) Foil. *Adv. Mater.* **2018**, *30*, 1706504.
36. Perera, H.A.; Raviranga, N.G.H.; Ramstrom, O.; Yan, M. Trehalose-Functionalized Magnetic Affinity Probe Provides Biochemical Evidence of Nanoparticle Internalization in Mycobacteria. *ACS Infect. Dis.* **2025**, *11*, 2847–2858.
37. Tu, J.; Zhou, W.; Kiani, A.; Wolf, L.M.; Yan, M. Chemical Vapor Deposition of Monolayer Graphene on Centimeter-Sized Cu(111) for Nanoelectronics Applications. *ACS Appl. Nano Mater.* **2025**, *8*, 4926–4939.
38. Yang, X.; Yan, M. Removing contaminants from transferred CVD graphene. *Nano Res.* **2020**, *13*, 599–610.
39. Ferrari, A.C.; Basko, D.M. Raman spectroscopy as a versatile tool for studying the properties of graphene. *Nat. Nanotechnol.* **2013**, *8*, 235–246.
40. Cancado, L.G.; Jorio, A.; Ferreira, E.H.; Stavale, F.; Achete, C.A.; Capaz, R.B.; Moutinho, M.V.; Lombardo, A.; Kulmala, T.S.; Ferrari, A.C. Quantifying defects in graphene via Raman spectroscopy at different excitation energies. *Nano Lett.* **2011**, *11*, 3190–3196.
41. Lucchese, M.M.; Stavale, F.; Ferreira, E.M.; Vilani, C.; Moutinho, M.d.O.; Capaz, R.B.; Achete, C.A.; Jorio, A. Quantifying ion-induced defects and Raman relaxation length in graphene. *Carbon* **2010**, *48*, 1592–1597.
42. Lee, J.E.; Ahn, G.; Shim, J.; Lee, Y.S.; Ryu, S. Optical separation of mechanical strain from charge doping in graphene. *Nat. Commun.* **2012**, *3*, 1024.

43. Wang, Q.H.; Jin, Z.; Kim, K.K.; Hilmer, A.J.; Paulus, G.L.; Shih, C.J.; Ham, M.H.; Sanchez-Yamagishi, J.D.; Watanabe, K.; Taniguchi, T.; et al. Understanding and controlling the substrate effect on graphene electron-transfer chemistry via reactivity imprint lithography. *Nat. Chem.* **2012**, *4*, 724–732.
44. Wu, Q.; Wu, Y.; Hao, Y.; Geng, J.; Charlton, M.; Chen, S.; Ren, Y.; Ji, H.; Li, H.; Boukhvalov, D.W.; et al. Selective surface functionalization at regions of high local curvature in graphene. *Chem. Commun.* **2013**, *49*, 677–679.
45. Deng, S.; Rhee, D.; Lee, W.K.; Che, S.; Keisham, B.; Berry, V.; Odom, T.W. Graphene Wrinkles Enable Spatially Defined Chemistry. *Nano Lett.* **2019**, *19*, 5640–5646.
46. Giovannetti, G.; Khomyakov, P.A.; Brocks, G.; Karpan, V.V.; van den Brink, J.; Kelly, P.J. Doping graphene with metal contacts. *Phys. Rev. Lett.* **2008**, *101*, 026803.
47. Kong, L.; Bjelkevig, C.; Gaddam, S.; Zhou, M.; Lee, Y.H.; Han, G.H.; Jeong, H.K.; Wu, N.; Zhang, Z.; Xiao, J. Graphene/substrate charge transfer characterized by inverse photoelectron spectroscopy. *J. Phys. Chem. C* **2010**, *114*, 21618–21624.
48. Khomyakov, P.; Giovannetti, G.; Rusu, P.; Brocks, G.V.; Van den Brink, J.; Kelly, P.J. First-principles study of the interaction and charge transfer between graphene and metals. *Phys. Rev. B.* **2009**, *79*, 195425.
49. Chen, C.; Avila, J.; Asensio, M.C. Chemical and electronic structure imaging of graphene on Cu: A NanoARPES study. *J. Phys. Condens. Matter* **2017**, *29*, 183001.
50. Zhou, L.; Liao, L.; Wang, J.; Yu, J.; Li, D.; Xie, Q.; Liu, Z.; Yang, Y.; Guo, X.; Liu, Z. Substrate-Induced Graphene Chemistry for 2D Superlattices with Tunable Periodicities. *Adv. Mater.* **2016**, *28*, 2148–2154.
51. Cullen, W.G.; Yamamoto, M.; Burson, K.M.; Chen, J.-H.; Jang, C.; Li, L.; Fuhrer, M.S.; Williams, E.D. High-fidelity conformation of graphene to SiO 2 topographic features. *Phys. Rev. Lett.* **2010**, *105*, 215504.
52. Li, T.; Zhang, Z. Substrate-regulated morphology of graphene. *J. Phys. D Appl. Phys.* **2010**, *43*, 075303.
53. Zhang, Y.; Heiranian, M.; Janicek, B.; Budrikis, Z.; Zapperi, S.; Huang, P.Y.; Johnson, H.T.; Aluru, N.R.; Lyding, J.W.; Mason, N. Strain modulation of graphene by nanoscale substrate curvatures: A molecular view. *Nano Lett.* **2018**, *18*, 2098–2104.
54. Negrito, M.; Elinski, M.B.; Hawthorne, N.; Pedley, M.P.; Han, M.; Sheldon, M.; Espinosa-Marzal, R.M.; Batteas, J.D. Using Patterned Self-Assembled Monolayers to Tune Graphene–Substrate Interactions. *Langmuir* **2021**, *37*, 9996–10005.